JACS
JOURNAL OF THE AMERICAN CHEMICAL SOCIETY
Article
pubs.acs.org/JACS

Quantification of Electrophilic Activation by Hydrogen-Bonding Organocatalysts

Ryan R. Walvoord, Phuong N. H. Huynh, and Marisa C. Kozlowski*

Roy and Diana Vagelos Laboratories, Department of Chemistry, University of Pennsylvania, Philadelphia, Pennsylvania 19104, United States

Supporting Information

ABSTRACT: A spectrophotometric sensor is described that provides a useful assessment of the LUMO-lowering provided by catalysts in Diels–Alder and Friedel–Crafts reactions. A broad range of 33 hydrogen-bonding catalysts was assessed with the sensor, and the relative rates in the above reactions spanned 5 orders of magnitude as determined via ^{1}H- and ^{2}H NMR spectroscopic measurements, respectively. The differences between the maximum wavelength shift of the sensor with and without catalyst ($\Delta\lambda_{max}^{-1}$) were found to correlate linearly with ln(k_{rel}) values for both reactions, even though the substrate feature that interacts with the catalyst differs significantly (ketone vs nitro). The sensor provides an assessment of both the *inherent reactivity* of a catalyst architecture as well as the *sensitivity* of the reaction to changes within an architecture. In contrast, catalyst pK_a values are a poor measure of reactivity, although correlations have been identified within catalyst classes.

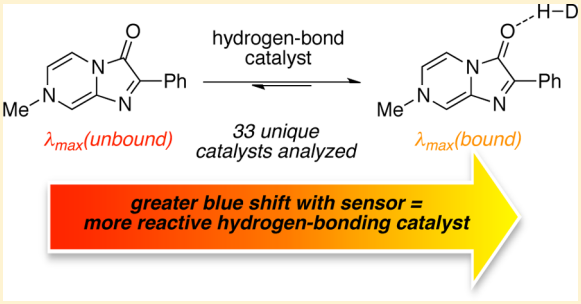

1. INTRODUCTION

The field of small-molecule organocatalysis via noncovalent interactions has seen rampant growth over the past decade.[1] This area, which aims to mimic the mechanisms used by nature in enzyme catalysis, is attractive due to its potential for high catalyst tunability and substrate specificity, as well as obviating the use of metals. While such research has resulted in many catalysts operating through bifunctional mechanisms,[2] the primary interaction responsible for electrophile activation occurs through hydrogen-bonding to an acceptor moiety. The consequent LUMO-lowering results in rate enhancement. In comparison to metal-based systems (i.e., Lewis Acids),[3−5] current metrics to estimate the reactivity of hydrogen bonding catalysts are ineffective. Although ΔpK_a values of the donor and acceptor may be used to infer hydrogen-bond strengths,[6] this analysis fails to account for several important secondary interactions, including sterics, dual-activation, and binding geometry.[7] As a result, the discovery of reactions compatible with hydrogen-bond catalysis is far outpacing understanding of catalyst interaction and mechanism. Indeed, while certain privileged organocatalyst motifs have been identified to be successful for several reaction types, rational design of these structures remains limited, relying on trial and error to achieve optimal reactivity and selectivity.

In a previous communication,[8] we described preliminary results showing the utility of small organic chromophore **S** for the detection of hydrogen-bonding interactions by UV–vis spectroscopy for a small set of catalysts (Scheme 1). Herein, we assess the general utility of this colorimetric sensor as a predictive gauge for the relative reactivity of a broad range of organocatalysts, including several widely used motifs, with the goal of encompassing many different hydrogen-bonding arrays. An additional goal was to validate the sensor measurements across significantly different reaction profiles, particularly those involving noncarbonyl electrophiles. The lack of comprehensive rate data for a range of catalysts in different reactions is a barrier to understanding the factors controlling catalytic activation. As a consequence, the relative rates have been measured for an array of catalysts in two reactions with different groups that interact with the catalysts. The sensor signal has been analyzed with respect to reaction profile, catalyst structure, acidity, and acceptor preference. Our findings establish the sensor as a useful substrate "surrogate" for probing and gauging catalyst

Scheme 1. UV–Vis Sensor Concept To Detect Weak Interaction

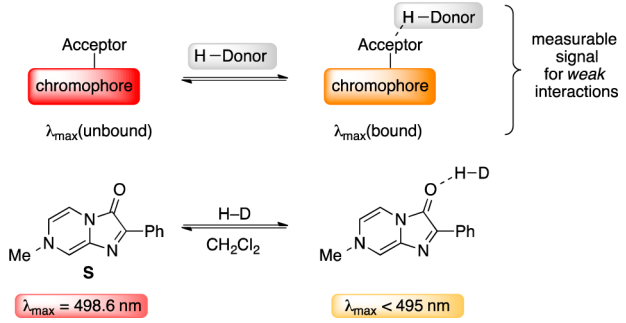

Received: August 21, 2014
Published: October 17, 2014

   dx.doi.org/10.1021/ja5086244 | J. Am. Chem. Soc. 2014, 136, 16055−16065

performance. Moreover, the data unequivocally establish that catalyst structure and binding mode are far more relevant to catalytic activity than acidity.

2. RESULTS AND DISCUSSION

2.1. Application of a Colorimetric Probe for Determining LUMO Activation. A key consideration in designing a method for measuring hydrogen-bond strengths is the very broad range of these noncovalent interactions (0.2−40 kcal/mol).[9] Observing the very weak range of these interactions is a challenge with commonly employed spectroscopic techniques. For example, despite successful application in measuring Lewis Acid binding effects,[10] preliminary NMR studies proved too insensitive for detecting the interactions of weak hydrogen-bonding catalysts with a carbonyl acceptor.[11]

We proposed an alternative approach using the sensitivity of UV−vis absorption profiles, in which a change in electronic excitation of an acceptor chromophore occurs upon binding to a hydrogen-bond donor (Scheme 1). Specifically, imidazopyrazinone **S** displays solvatochromism with protic solvents as well as color changes with a small number of Lewis Acids.[12] We postulated that upon treatment with various hydrogen-bond donors, the carbonyl moiety of **S** would act as an acceptor moiety. The resulting hydrogen-bonding interaction would alter the electronic transition of the chromophore, detectable by simple UV−vis spectroscopy.

In line with this reasoning, treatment of sensor **S** in dichloromethane with various hydrogen-bond donors resulted in visible hypsochromic (blue) shifts (Figure 1). Importantly,

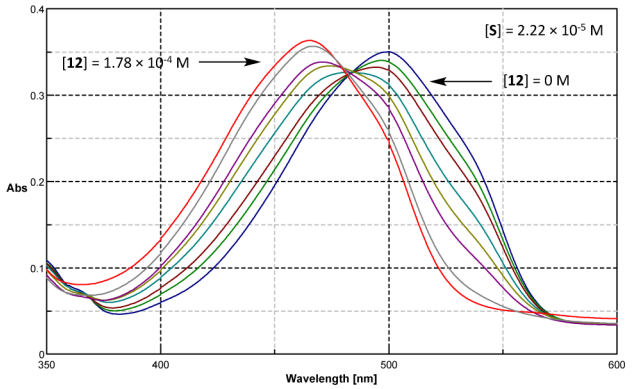

Figure 1. Response in the UV−vis spectrum of **S** upon increasing amounts of **12**. [**S**] = 2.22 × 10^{-5} M in CH_2Cl_2, [**12**] = 0 to 1.78 × 10^{-4} M.

compounds anticipated to be weaker donors, such as diphenylthiourea (**1**), yielded significant changes in sensor signal. Variation of binder concentration resulted in titration-like behavior, with a measurable end point upon saturation of sensor with catalyst. An array of catalysts (Chart 1), varying in structure and anticipated strength, was examined with the colorimetric sensor, and the $\Delta\lambda_{max}$ upon saturation was determined.

DFT molecular orbital calculations were performed on bound and unbound sensor for selected hydrogen-bonding agents to gauge the orbital perturbation (Table 1). The calculated lowest energy transition accurately predicts the observed absorbance maximum for the free sensor. More importantly, the HOMO−LUMO energy gap was larger for all bound complexes, in accord with the empirically observed hypsochromic shift in Figure 1. An increased shift (lower λ_{max}) is predicted for binders of ostensibly greater strength (e.g., proton > benzoic acid > phenol).

The UV absorption behavior of the sensor with the hydrogen-bonding agent can be represented as shown in Figure 2a. The lowest energy electronic transition may be ascribed to the n (HOMO) to π^* (LUMO) transition, ΔE_1, corresponding to the measured λ_{max}. As supported by the above calculations, addition of a hydrogen-bonding agent stabilizes the ground state (HOMO) to a greater extent than the excited state (LUMO), i.e., $\Delta E_3 > \Delta E_2$. As a consequence, a hypsochromic shift is observed upon interaction of the sensor with the hydrogen-bond donors. For comparison, Figure 2b illustrates the energy diagram for a typical reaction with a hydrogen-bonding catalyst, in which catalysis is effected by LUMO-lowering of the electrophile (ΔE_a). We hypothesized that $\Delta E_3 - \Delta E_2$ is proportional to ΔE_a, i.e., the wavelength shift of the bound sensor•catalyst is proportional to the rate enhancement afforded in a reaction with the hydrogen-bonding catalyst.

2.2. Correlation of Binding with Sensor Wavelength Shift. As shown in Figure 1, a continuous wavelength shift was revealed upon saturation of the sensor with the catalyst. The lack of two distinct peaks in intermediate measurements containing both bound and unbound sensor indicates a rapid equilibration. Thus, plots of absorbance vs [catalyst] (see Figure 3 for an example with bisamidinium **12**) were used to determine the binding constants (K_{eq}) for the sensor•catalyst complex. A significant range of blue shifts was observed for the different catalyst donors, ranging from ∼490 to 465 nm ($\Delta\lambda_{max}$ ∼10−30 nm). In general, catalysts with larger $\Delta\lambda_{max}$ values possessed much stronger binding constants. Since ΔE_1 is proportional to $1/\lambda_{max}$, the energetics of the interaction of the sensor with the catalysts ($\Delta E_3 - \Delta E_2$) is proportional to $1/\lambda_{max}$(sensor•catalyst) − $1/\lambda_{max}$(sensor). Indeed, a good correlation of this inverse wavelength shift with ln(K_{eq}) was found (Figure 4). Note that in this plot, both axes are linearly proportional to energy terms: $\Delta\lambda^{-1}$ to the ΔE of the sensor electronic absorption, and ln(K_{eq}) to ΔG of sensor•catalyst formation. Importantly, this relationship establishes the observed wavelength shift as a reliable gauge for binding affinity of a catalyst to the sensor molecule.

Using the sensor•catalyst wavelength shift as predictors of catalyst reactivity yields several noteworthy observations. Diol-based **30** (TADDOL) and silanol catalysts **31** and **32** afforded very weak shifts, despite application in numerous transformations, including Rawal's seminal report on the asymmetric hetero Diels−Alder reaction.[14] The greater λ_{max} shift of **32** compared to the related monosilanol **31** mirrors the increased reactivity of this silanediol scaffold, as elegantly reported by Mattson[15] and Franz.[16,17] Benzoic acids and phenols spanned the intermediate range of sensor shifts, with trends clearly based on the electronic effects of aromatic substitution. Although these structures are not as commonly incorporated as hydrogen-bond catalysts, Schafmeister and co-workers have recently demonstrated the spiroligozyme catalyst **24**, containing a carefully arranged carboxylic acid and phenol, as an effective ketosteroid isomerase mimic for the aromatic Claisen rearrangement.[18] *N*,*N*′-Diaryl thioureas and ureas, particularly those with multiple trifluoromethyl substituents such as Schreiner's catalyst **4**,[19] afforded some of the largest sensor shifts, indicative of the immense utility of these structures in various organocatalysts.[20] The internally activated BF_2-urea **9**

dx.doi.org/10.1021/ja5086244 | J. Am. Chem. Soc. 2014, 136, 16055−16065

Chart 1. Hydrogen-Bonding Catalyst Structures Investigated

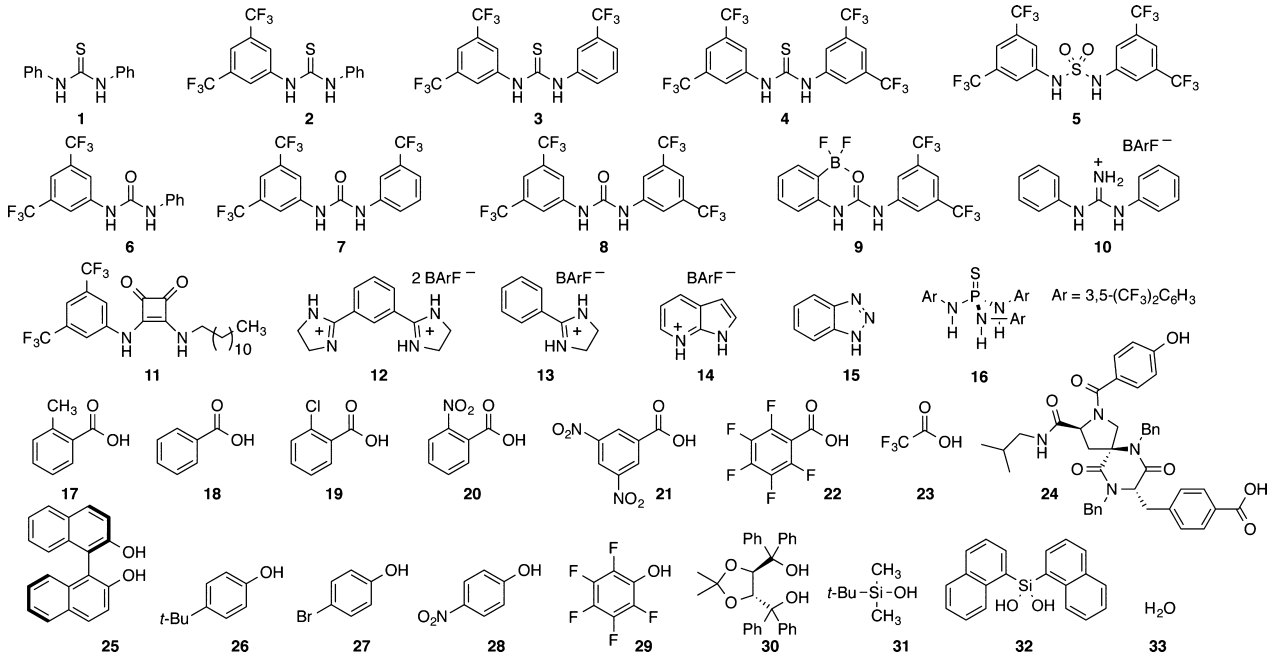

Table 1. Calculated HOMO−LUMO Energies for Bound and Unbound Sensor Complexes[a]

binder	HOMO (eV)	LUMO (eV)	HOMO−LUMO (eV)	Calculated λ_{max} (nm)
-	−4.23	−1.68	2.55	487
phenol	−5.11	−2.18	2.92	425
$PhCO_2H$	−5.08	−2.02	3.05	407
proton	−9.43	−6.08	3.35	370

[a]Energies obtained from B3LYP/6-31G(d) optimized structures.

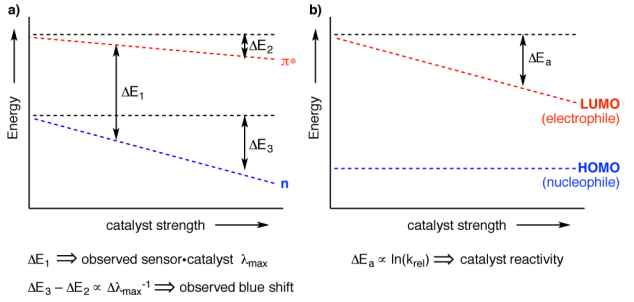

Figure 2. (a) Proposed energy diagram of the lowest energy electronic transition of the sensor upon interaction with catalysts of increasing strength, corresponding to the hypsochromic wavelength shift ($\Delta\lambda_{max}$). (b) LUMO-lowering of reactants via hydrogen-bonding catalysts, corresponding to increased reaction rates (k_{rel}).

provided the largest shift within this class, in line with experimental reactivity data reported by Mattson and co-workers.[21] Finally, formally cationic species, including guanidinium, amidinium, and Takenaka's azaindolium **14**[22] were the strongest binders, with wavelength shifts ranging from 26 to 34 nm (λ_{max} = 473−465 nm). Interestingly, one of the strongest noncationic binders was thiophosphoramide **16**, possessing a pocket of three potential N−H donors. To date, this array has seen only limited use in organocatalysis.[23,24] Squaramide-containing scaffolds have yielded excellent results as hydrogen-bond activators;[2a,25] however, these compounds possess limited

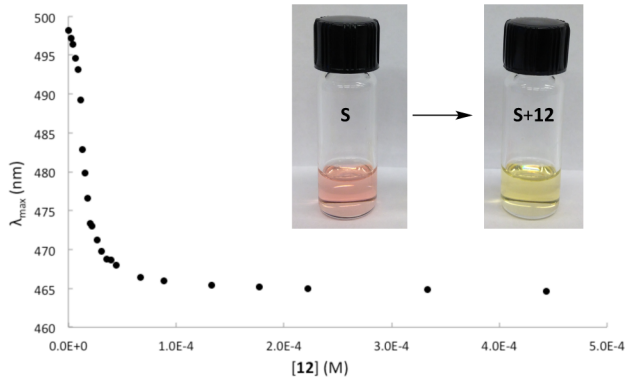

Figure 3. UV-titration curve of catalyst **12** in CH_2Cl_2 using [**S**] = 2.22 × 10^{-5} M. Inlay: visible color change of sensor before (red) and after addition of **12** (yellow; [**12**] = 1.78 × 10^{-4} M).

solubility, and are typically employed as heterogeneous catalysts. Representative squaramide **11**, containing the common *N*-3,5-$(CF_3)_2$aryl and *N*′-alkyl array, was synthesized, and gave an apparent sensor end point of ∼480 nm. Due to its relative insolubility, an accurate binding equilibrium value could not be determined.

It is worth noting the experimental ease with which the sensor metric can be obtained. Compound **S** itself is easily obtained in 2 steps from commercial materials,[12a,26] and very little sensor or catalyst (particularly for strong catalysts) is necessary to obtain the wavelength shift. The titration experiment is largely insensitive to moisture, as illustrated by the poor binding observed in the sensor titration with water.

Applying the method of continuous variation to the sensor with catalyst **12** revealed a 1:1 binding stoichiometry with the sensor molecule (Figure 5).[13] This observation is significant, since several other binding situations may be postulated, including donation of one catalyst molecule to several sensors (4 equivalent N−H bonds on **12**, for example).

Benzoic acids and phenols offer useful templates to study electronic effects on sensor signal due to availability and well-

dx.doi.org/10.1021/ja5086244 | J. Am. Chem. Soc. 2014, 136, 16055−16065

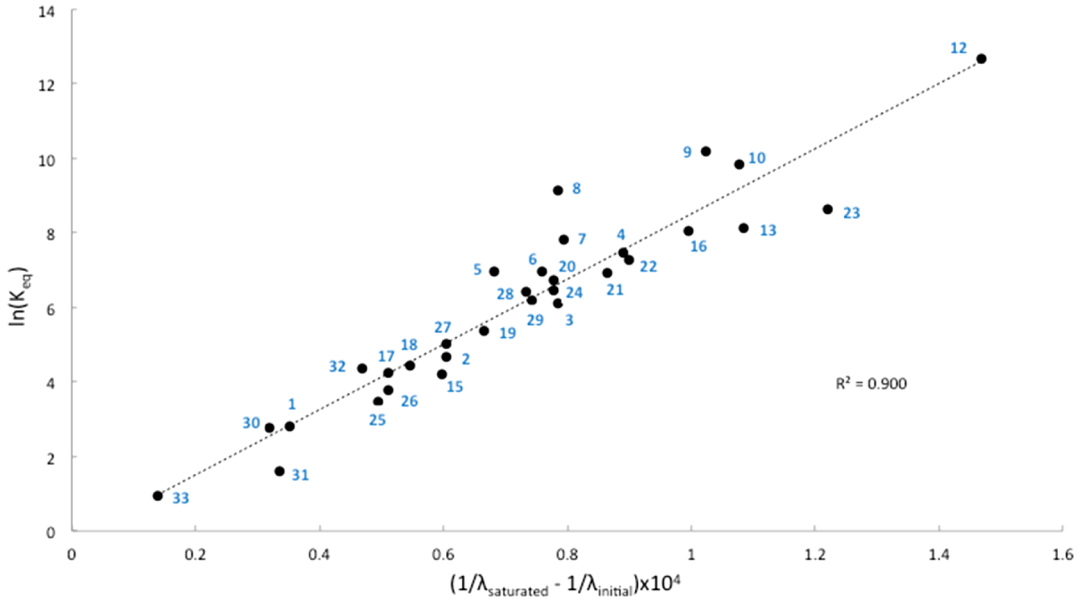

Figure 4. Correlation between sensor wavelength shift and sensor•catalyst binding equilibrium constant. All titrations were performed with [S] = 2.22×10^{-5} M in CH_2Cl_2.[13]

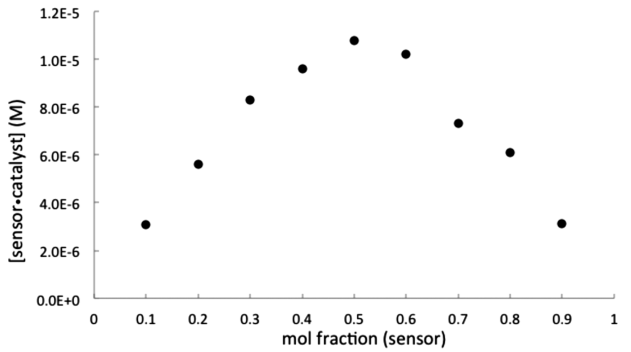

Figure 5. Job plot analysis of catalyst **12** with sensor **S** showing 1:1 binding stoichiometry.

understood behavior of aromatic substitution. Due to solubility limitations, *ortho*-substituted benzoic acids were studied rather than the *para*-substituted analogs. The electronic effects from substitution on the sensor interaction can be illustrated via a Hammett-type plot, as shown in Figure 6. As may be anticipated from the Brønsted catalysis law (see Section 2.6 for further discussion), increasingly electron-withdrawing substituents on these structures correlate with larger hypsochromic shifts of the sensor•catalyst complex. For both catalyst sets, highly linear relationships are evident with substituent σ parameters indicating that the wavelength shift provides an accurate readout of electronic perturbation on the hydrogen-bonding ability.

Notably, the wavelength shifts seen with the sensor do not correspond directly with pK_a either in water (Figure 7a, R^2 = 0.0007) or DMSO (Figure 7b, R^2 = 0.0950). However,

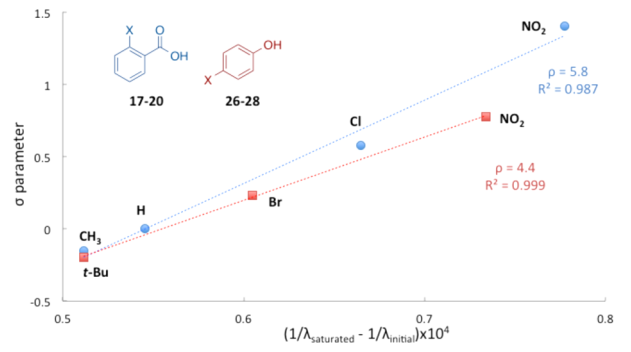

Figure 6. Correlation of Hammett σ parameters for *o*-benzoic acids (σ_{ortho}^{i})[27] and *p*-phenols (σ_{para}) with sensor•catalyst wavelength shifts.

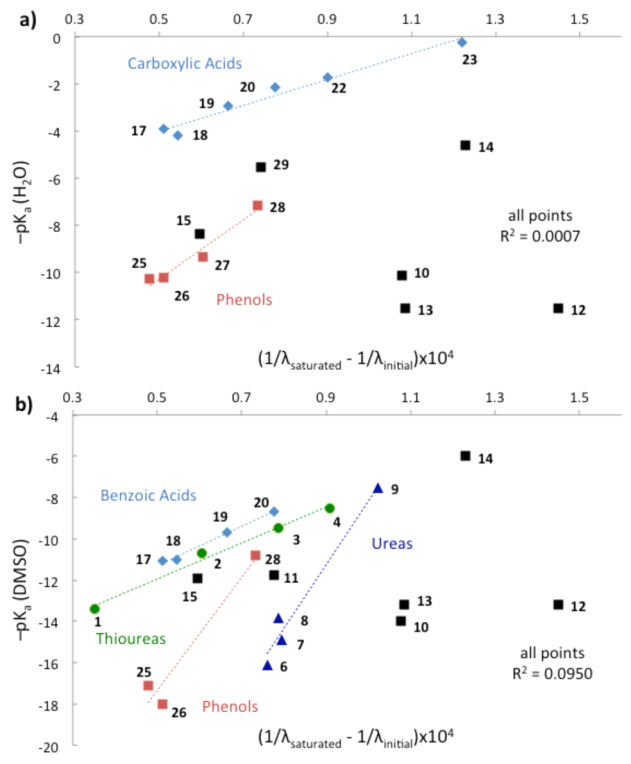

Figure 7. Plot of catalyst acidity in water (a) or DMSO (b) vs sensor•catalyst wavelength shifts. Correlation is only observed within closely related catalyst groups.

dx.doi.org/10.1021/ja5086244 | J. Am. Chem. Soc. 2014, 136, 16055−16065

correlations are observed for closely related catalyst structures, wherein electronic perturbations modify the acidity of the donor moiety without introducing significant secondary effects. This observation provides potential for the sensor to estimate pK_a values within a series of related compounds. Persubstituted phenol **29** deviates from other phenolic catalysts, which may be attributed to the increased steric demand around the donating O–H bond.

The correlation of the observed blue shift with the binding strength across a large range of hydrogen-bond donors proved the metric to be able to quantitatively detect these interactions. However, this finding does *not* necessitate a correlation with catalyst reactivity. In order for this correlation to occur, the sensor must be a good facsimile of the substrate that is undergoing reaction. Other factors, including alternate binding modes and steric effects, might come into play when a substrate interacts with hydrogen-bonding agent in a catalyzed reaction.

2.3. Comparison of Sensor Shifts with Hydrogen-Bond Catalyzed Diels–Alder Rate Data. To be a useful metric for the community, the sensor signal must correlate to empirically obtained rate enhancement via hydrogen-bond catalysis (Scheme 2). Myriad reaction profiles have been

Scheme 2. Sensor as a Surrogate for an Electrophilic Substrate

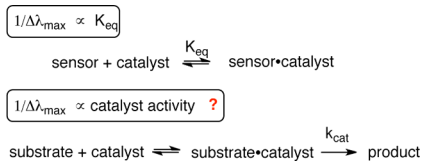

reported that are established to proceed via hydrogen-bond activation of the electrophile (LUMO-lowering activation). In order to best isolate the reactivity enhancement offered by the catalysts strictly due to hydrogen-bonding, we first targeted a reaction where the electrophile has only one possible point of interaction with the catalyst, and the nucleophile does not contain binding points (i.e., no heteroatoms). Additionally, the reaction should have minimal background rate and a method to easily analyze starting material and/or product concentrations.

The reaction of methyl vinyl ketone (MVK) with cyclopentadiene (Cp) offers a useful reaction platform that fulfills these criteria (Scheme 3), and has been used to gauge the

Scheme 3. Diels–Alder Kinetic Study via ^{1}H NMR

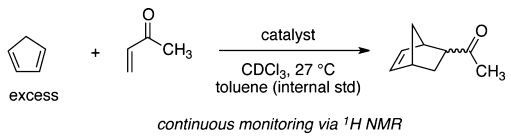

relative strength of thiourea[19a] and bisphenol[7b] catalysts previously. Hydrogen-bonding to the ketone carbonyl accounts for catalysis in this reaction. Importantly, the binding in the sensor•catalyst complex is very similar to that of the MVK•catalyst intermediate as both interactions arise from a carbonyl acting as a hydrogen-bond acceptor.

Systematic investigation of the Diels–Alder reaction of MVK and Cp with a variety of catalysts was performed under pseudo-first order conditions as described in Scheme 3. Kinetic data was acquired via continuous sampling (5 min intervals) by ^{1}H NMR spectroscopy, and each rate measurement was performed in triplicate. Relative rate constants, k_{rel}, were calculated as described in eq 1 from the observed pseudo-first order rate constant k'_{obs} and background rate $k_{background}$, and were normalized for catalyst concentration N. The resulting values directly provide the rate enhancement afforded by the catalyst.

$$k_{rel} = \left(\frac{k'_{obs} - k_{background}}{k_{background}} \right) N \quad (1)$$

As displayed in Figure 8, a plot of $\ln(k_{rel})$ against the inverse sensor wavelength shift of 18 catalysts shows an excellent

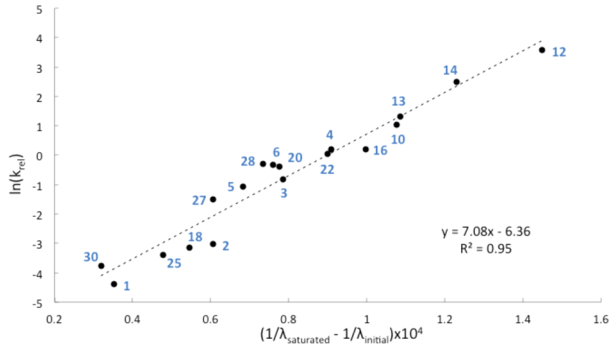

Figure 8. Correlation between the sensor•catalyst wavelength shift and catalyst rate enhancement in the Diels–Alder reaction between MVK and Cp.

correlation. Catalysts with greater blue shifts when treated with the sensor show greater activity in the Diels–Alder reaction via correspondingly greater LUMO lowering of the ketone in the dienophile. More precisely, the change in energy of the sensor upon binding with the catalyst is proportional to the change in activation energy of the hydrogen-bond catalyzed Diels–Alder reaction.

The observed correlation establishes that, at least in this class of reaction, the sensor signal is a good indicator of LUMO-lowering ability of these small molecules as hydrogen-bond catalysts. Importantly, the results also indicate that the binding interaction of the sensor with catalysts is similar to that of methyl vinyl ketone with catalyst, i.e. the sensor is a useful gauge of carbonyl activation.

2.4. Comparison of Sensor Shifts with Hydrogen-Bond Catalyzed Friedel–Crafts Rate Data. The addition of various nucleophiles into nitroalkenes is one of the most widely used reaction motifs in hydrogen-bonding catalysts; it is often used as a measure of reactivity when developing and comparing novel catalyst structures.[7d,15a,16,21a,22,28] To test the effectiveness of our sensor metric beyond the Diels–Alder reaction, we studied the Friedel–Crafts addition of *N*-methylindole (**34**) into nitrostyrene **35** (Scheme 4). Deuterated **35** was easily prepared via Henry condensation using d_3-nitromethane with the corresponding aldehyde. Again, the number of hydrogen

Scheme 4. Friedel–Crafts Kinetic Study via ^{2}H NMR

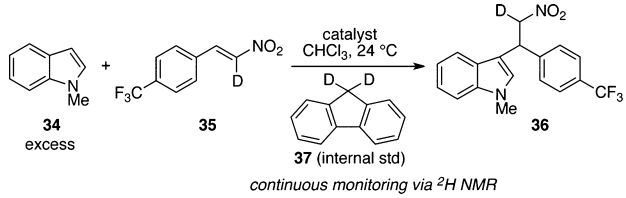

dx.doi.org/10.1021/ja5086244 | J. Am. Chem. Soc. 2014, 136, 16055–16065

bond acceptors is limited in this reaction. Nucleophile **34** provides a reasonably active coupling partner while minimizing potential catalyst interactions [pK_a(H_2O) *N*-methylindolium = −1.8].[29] Thus, the effects of hydrogen bonding catalysts on the activation of the styrene electrophile via binding to the nitro acceptor can be cleanly delineated.

Significantly, the catalyzed rates of this reaction allow comparison of the effects of hydrogen-bonding catalysts on carbonyl acceptors (the sensor and MVK) versus nitro acceptors (nitrostyrene **35**) as outlined in Scheme 5. While

Scheme 5. Catalyst−Acceptor Binding for Sensor and Reaction Electrophiles

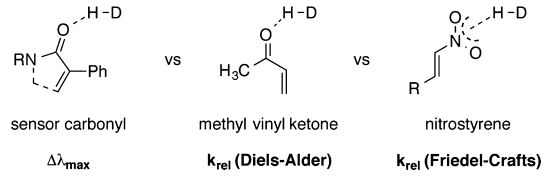

binding geometries to carbonyl groups are anticipated to be similar, an analogous correlation may not be automatically presumed for a nitro group. In particular, the nitro group contains a formally delocalized negative charge across three atoms, and has been suggested to form κ^2-activated intermediates with certain catalyst structural types such as squaramides and thioureas.[21b,f,30]

As illustrated in Figure 9, kinetic reaction data was acquired using ^{2}H NMR spectroscopy. Although initial ^{1}H NMR spectroscopic studies with proteo-**35** provided usable data,

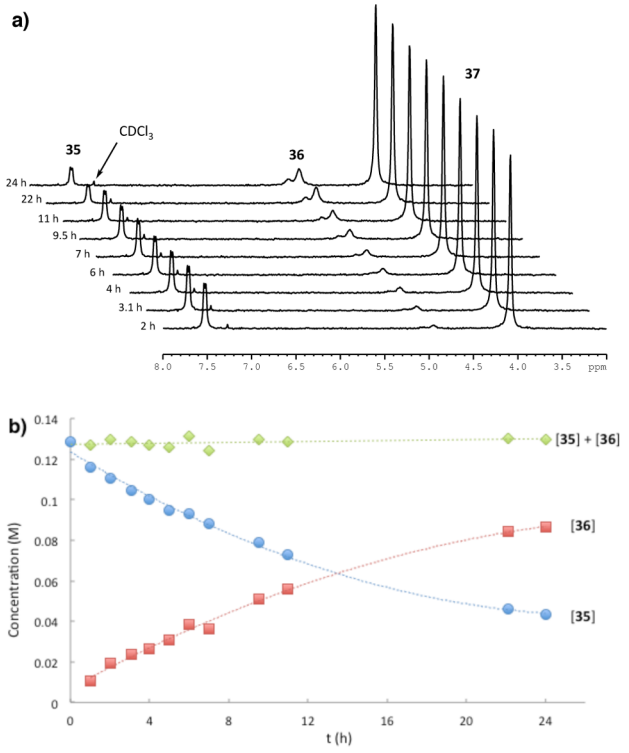

Figure 9. (a) Stacked ^{2}H NMR plot and (b) kinetic profile for the Friedel−Crafts reaction shown in Scheme 4 using catalyst **12**. Conditions: [**34**] = 1.33 M, [**35**] = 0.133 M, [**37**] = 0.133 M, [**12**] = 2.67 × 10^{-4} M. The $CDCl_3$ peak arises from natural abundance in $CHCl_3$.

employment of a deuterium label provides exceptional signal isolation. Moreover, overlap of signals from the catalyst is completely mitigated, since only substrate, product, and internal standard exhibit appreciable resonances. As a result, *any catalyst can be readily analyzed.*

The Friedel−Crafts reaction was studied under pseudo-first order conditions using the broad series of hydrogen-bond catalysts shown in Chart 1. The relative catalytic strength of each catalyst was calculated according to eq 1, using averaged k'_{obs} values from duplicate trials. A plot of ln(k_{rel}) and inverse sensor wavelength shift is shown in Figure 10a. Similar to the

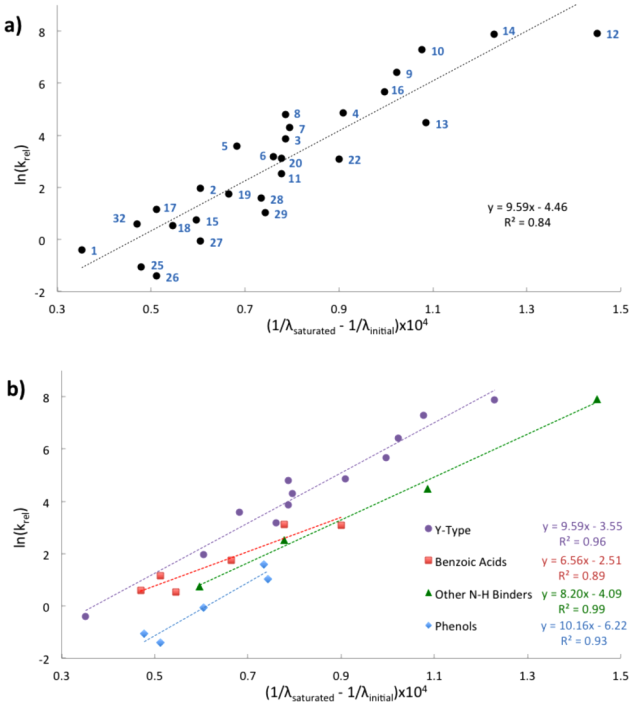

Figure 10. (a) Correlation observed between the sensor•catalyst wavelength shift and catalyst rate enhancement in the Friedel−Crafts reaction. (b) Correlations based on catalyst structure groups.

Diels−Alder reaction, and predicted based on sensor shifts, cationic binders proved to be the most effective catalysts, followed by electron-deficient ureas and thioureas. Squaramide **11**, employed here as a heterogeneous catalyst, provided moderate rate enhancement as predicted by its sensor wavelength shift. Thiophosphoramide **16** and sulfonamide **6** have previously been studied in a Friedel−Crafts reaction under nearly identical conditions by Shea and co-workers.[23a] The k_{rel} values reported for these catalysts and **4** align closely with the values measured in this work.

The overall correlation of the sensor wavelength shift with catalyst strength for the Friedel−Crafts reaction is good (R_2 = 0.84), but not as strong as that found in the Diels−Alder reaction (R_2 = 0.95). Analysis of this data suggests that the binding interaction of a hydrogen-bonding catalyst with the sensor carbonyl does not fully mimic that of a hydrogen-bonding catalyst with the activated nitroalkene. Closer inspection reveals that the wavelength shift is correlated even more strongly to catalyst strength *within an isostructural catalyst series* (Figure 10b). Specifically, the catalysts can be placed in four groups based on their general structure: benzoic acids, phenols, "Y-type" binders, and other N−H binders. The Y-type

dx.doi.org/10.1021/ja5086244 | J. Am. Chem. Soc. 2014, 136, 16055−16065

group consists of catalysts possessing two N−H donor groups separated by a single atom, such as ureas, thioureas, guanidines, bis-sulfonamides, etc. The other N−H binders include those catalysts that have more than one atom separating the donor array (squaramide **11**, bisamidinium **12**) or can only donate one N−H bond (benzotriazole **15**, monoamidinium **13**). Interestingly, the silanediol catalyst **32** exhibits reactivity falling nicely in line with benzoic acids, possibly due to a similar O−H geometry. This analysis quantitatively shows that Y-type structures are superior for nitroalkene activation. In contrast, phenols provided the least activation relative to their binding interaction with the sensor.

Overall, the sensor provides a good assessment of relative reactivity of hydrogen-bond catalysts in the Friedel−Crafts reaction. The presence of stronger correlations within catalyst structural classes is consistent with some catalysts activating nitroalkenes via a different mode (e.g., κ^2-binding) that is not completely captured by the interactions of the catalysts with the carbonyl of the sensor molecule. This analysis underlines the complex nature of hydrogen-bonding, emphasizing that caution must be exercised in generalizing catalyst reactivity or selectivity from one reaction to another.

2.5. Unified Description of Reactivity versus Sensor Measurements. A general equation to describe catalyst strength for reaction r based on sensor response ($\Delta\lambda^{-1}$) is presented in eq 2. Parameter R_r (slope) represents the *responsiveness* of the rate per unit catalyst strength as determined by the sensor measurement. Parameter C_r (y-intercept) corresponds to inherent *complementarity* of the catalyst to the electrophilic reaction partner.

$$\text{Catalyst Reactivity} \propto \ln(k_{rel}) = R_r\Delta(\lambda^{-1}) + C_r \quad (2)$$

The parameter values (Table 2) for the reactions shown in Scheme 3 (Diels−Alder) and Scheme 4 (Friedel−Crafts) were

Table 2. Reaction Coefficients for Equation 3

reaction	R	C
Diels−Alder	7.08	−6.36
Friedel−Crafts	9.59	−4.46

obtained using the kinetic data from Figures 8 and 10, respectively. Comparison of the R_{DA} and R_{FC} values reveals that the Friedel−Crafts is more sensitive to catalyst strength. In other words, the same catalyst produces a greater relative rate enhancement for the Friedel−Crafts reaction than for the Diels−Alder reaction. Similarly, a given wavelength shift of the sensor by a catalyst will cause a greater reactivity change in the Friedel−Crafts vs the Diels−Alder reaction. On the other hand, the C_{DA} and C_{FC} values indicate the inherent *complementarity* of the electrophilic substrate with catalysts; greater *complementarity* translates to greater reactivity. Notably, the C values represent reactivity when there is no wavelength shift (no perturbation of the sensor by the catalysts) and represent the lower limit of LUMO activation afforded by the catalyst.

Catalyst group-specific coefficients r_r and c_r can be introduced (eq 3) to account for variation if the sensor binds the catalyst differently than the reaction electrophile. Due to the strong correlation of the sensor shift to relative rates independent of catalyst structure, coefficients are unnecessary for the Diels−Alder reaction ($r_{DA} \approx c_{DA} \approx 1$). As discussed in Section 2.4, the sensor does not completely model catalyst binding to the nitrostyrene acceptor of the Friedel−Crafts reaction. Accordingly, the slope and intercept data from Figure 10b were combined with the R and C values from Table 2 to afford coefficient values for r_{FC} and c_{FC}, respectively, as provided in Table 3.

$$\ln(k_{rel}) = r_rR_r\Delta(\lambda^{-1}) + c_rC_r \quad (3)$$

Table 3. Catalyst Structure Coefficients for Friedel−Crafts Catalysis

catalyst series	r_{FC}	c_{FC}
Y-type	1.00	0.80
Benzoic Acids	0.68	0.56
Phenols	1.06	1.39
Other N−H Binders	0.86	0.92

The coefficient values in Table 3 reveal general trends between the different catalyst structural types and rate in the Friedel−Crafts reaction. Again, r_{FC} values are a measure of *responsiveness* of a given catalyst architecture to a perturbation in sensor binding. For Y-type and phenolic catalysts, r_{FC} is noticeably higher than the other N−H binders, and particularly benzoic acids. Thus, for the same amount of wavelength shift, the phenol and Y-type catalysts provide greater increases in reactivity relative to the other N−H binders and benzoic acids. This observation indicates that the sensor can assess electronic effects in a catalyst series. Comparison of the Hammett effects on $\Delta\lambda^{-1}$ (Figure 6; ρ_{acid} = 5.8, ρ_{phenol} = 4.4) with those on $\ln(k_{rel})$ (ρ_{acid} = 0.60, ρ_{phenol} = 0.33)[13] provides support for this assertion; both measures show a stronger electronic effect for the carboxylic acid series.

On the other hand, lower c_{FC} values indicate the inherent *complementarity* of a given catalyst architecture. For example, the Y-type binders activate nitro electrophiles to a greater extent at a given wavelength shift relative to phenols or the other N−H binders. Interestingly, the c_{FC} value for benzoic acids would predict high catalytic activity relative to Y-type binders, but only in the weak binding regime (left side of plot). Due to the low r_{FC} value for benzoic acids, the trends invert such that Y-type binders are superior in the strong binding regime (right side of plot). Considering both terms together, the Y-type binders are both more complementary to the nitroalkene and more efficient at LUMO lowering, thereby providing superior reactivity.

2.6. Comparison of Catalyst Reactivity and Acidity: Brønsted Analysis. Acidity values have widely been used as a guiding principle in hydrogen-bond catalyst design, under the premise that a more acidic donor will form a stronger interaction and stabilize the buildup of anionic charge in the transition state to a greater extent. Indeed, several reports have observed increased activity with judicious electronic tuning of the donor hydrogen.[17c,38] However, even ostensibly subtle changes to catalyst structure can cause secondary factors to override the reliability of pK_a as a predictive measure, as demonstrated by Cheng's recent study[39] on thiourea derivatives and even noted in the seminal work by Hine on mono- and bis-phenols.[40] Having proved the effectiveness of the sensor signal as a gauge for catalyst strength, we undertook a comparison with acidity to determine the similarities and differences between the two metrics.

Aggregate data for all catalysts spanning 3 orders of magnitude in reactivity for the Diels−Alder reaction and 4 orders in the Friedel−Crafts reaction is organized by increasing

dx.doi.org/10.1021/ja5086244 | J. Am. Chem. Soc. 2014, 136, 16055−16065

Table 4. Sensor Shifts, Binding Constants, Relative Rate Data, and Acidity Values for Catalysts Investigated

catalyst	λ_{max} (nm)	K_{eq} (M^{-1})	k_{rel} (Diels–Alder)	k_{rel} (Friedel–Crafts)	pK_a (H_2O)	pK_a (DMSO)
H_2O (**33**)	495.2	2.54	-	-	15.75[a]	32[a]
(*R*,*R*)-TADDOL (**30**)	490.8	1.57×10^1	0.023	-	~16	28–30[b]
TBDMSiOH (**31**)	490.4	4.87	-	-	~12[c]	-
Diphenylthiourea (**1**)	490.0	1.67×10^1	0.012	0.68	-	13.4[d]
Silanediol (**32**)	487.2	7.88×10^1	-	1.82	11.8[c]	-
(*R*)-BINOL (**25**)	487.0	3.18×10^1	0.034	0.35	10.28[e]	17.1[e,f]
4-*t*-Bu-phenol (**26**)	486.2	4.30×10^1	-	0.25	10.23[g]	~18[a]
2-Me-BzOH (**17**)	486.2	7.04×10^1	-	3.21	3.91[g]	11.07[h]
BzOH (**18**)	485.4	8.35×10^1	0.086	1.72	4.20[g]	11.00[h]
Benzotriazole (**15**)	484.2	6.57×10^1	-	2.12	8.38[g]	11.9[a]
4-Br-phenol (**27**)	484.0	1.50×10^2	0.224	0.93	9.34[g]	-
$(CF_3)_2$-thiourea (**2**)	484.0	1.07×10^2	0.049	7.13	-	10.7[d]
2-Cl-BzOH (**19**)	482.6	2.15×10^2	-	5.81	2.94[g]	9.70[h]
Sulfonamide (**5**)	482.2	1.04×10^3	0.337	36.4	-	<12.9[a,i]
4-NO_2-phenol (**28**)	481.0	6.05×10^2	0.733	4.94	7.14[g]	10.8[a]
F_5-phenol (**29**)	480.8	4.92×10^2	-	2.82	5.53[j]	-
$(CF_3)_2$-urea (**6**)	480.4	1.05×10^3	0.724	24.1	-	16.1[d]
Squaramide (**11**)[k]	480.0	-	-	12.5	-	11.5–12.0[l]
Spiroligozyme (**24**)	480.0	6.30×10^2	-	-	4–5	-
2-NO_2–BzOH (**20**)	480.0	8.27×10^2	0.669	22.8	2.17[g]	8.66[h]
$(CF_3)_3$-thiourea (**3**)	479.8	4.52×10^2	0.442	47.0	-	9.5[d]
$(CF_3)_4$-urea (**8**)	479.8	9.38×10^3	-	120.0	-	13.8[d]
$(CF_3)_3$-urea (**7**)	479.6	2.52×10^3	-	73.4	-	14.9[d]
3,5-NO_2–BzOH (**21**)	478.0	1.02×10^3	-	-	-	-
F_5–BzOH (**22**)	477.2	1.41×10^3	1.04	22.2	1.75[m]	-
$(CF_3)_4$-thiourea (**4**)	477.0	1.77×10^3	1.22	130.6	-	8.5[d]
Thiophosphoramide (**16**)	475.0	3.11×10^3	1.23	291.1	-	-
BF_2-urea (**9**)	474.4	2.65×10^4	-	603.5	-	7.5[n]
Guanidinium (**10**)	473.2	1.84×10^4	2.81	1446	10.12[g]	14[o]
MonoAmidinium (**13**)	473.0	3.34×10^3	3.69	89.1	11–12[g]	12.8–13.6[p]
TFA (**23**)	470.0	5.49×10^3	-	-	0.23[g]	-
Azaindolium (**14**)	469.8	-	12.2	2604	4.6[g]	6[q]
BisAmidinium (**12**)	465.0	3.22 x10^5	35.1	2763	11–12[g]	12.8–13.6[p]
PPTS	-	-	0.190	72.7	5.2[a]	3.4[a]
Diphenylphosphate	-	-	0.951	26.9	1.29[g]	-
CSA	-	-	8.53	103.3	−0.6[a]	1.6[a]

[a]Ref 31. [b]Ref 32. [c]Ref 17c. [d]Ref 41. [e]Ref 33. [f]Value for 2-naphthol. [g]Ref 29. [h].Ref 27. [i]Value for the less acidic *N*-phenylmethanesulfonamide analogue. [j]Ref 34. [k]Titrations and reactions were performed heterogeneously. [l]Ref 42. [m]Ref 35. [n]Ref 38c. [o]Ref 36. [p]Ref 37. [q]Ref 22.

sensor wavelength shift in Table 4. Recent efforts by Schreiner[41] and others[42] provided accurate acidity values of common hydrogen-bond donors. The Brønsted catalysis equation (eq 4), which describes the relationship for the rate of an acid-catalyzed reaction with the pK_a of the acid,[43] was applied to this data.

$$\log(k) = \alpha \log(K_a) + b \quad (4)$$

Figures 11 and 12 display the results for selected catalyst series in the Diels–Alder and Friedel–Crafts reactions, respectively.[44] These plots prove the linear free energy relationships (LFERs)[45] between catalyst acceleration and acidity *among catalysts of very similar structure*. In general, these LFERs exhibited a narrow range of α values (0.39–0.47; Table 5), indicating a similar degree of hydrogen-bonding in the transition states and that these reactions are not proceeding through formal protonation (α = 1). Slightly higher values found for benzoic acids in the Diels–Alder (α = 0.57) indicate a greater degree of proton transfer in the transition states consistent with the ionic nature of benzoic acids. Lower values for ureas in the Friedel–Crafts (α = 0.31) indicate a lesser degree of proton transfer in the transition states in line with the covalent nature of the N–H bonds.

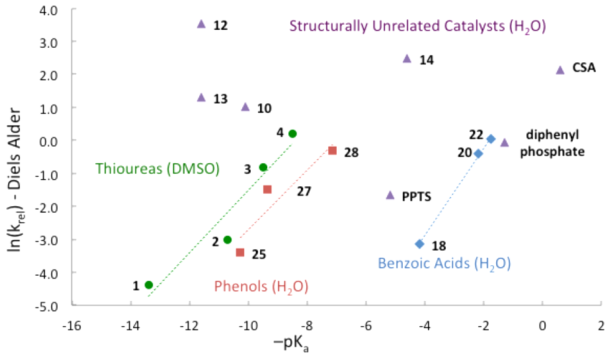

Figure 11. Brønsted catalysis plot for the Diels–Alder reaction, demonstrating LFERs for closely related catalyst groups.

More significantly, these figures clearly demonstrate the inherent limitations of estimating catalyst strength using acidity metrics. A pertinent example can be found in the thiourea and urea catalysts. Based solely on pK_a measurements, thioureas

dx.doi.org/10.1021/ja5086244 | J. Am. Chem. Soc. 2014, 136, 16055–16065

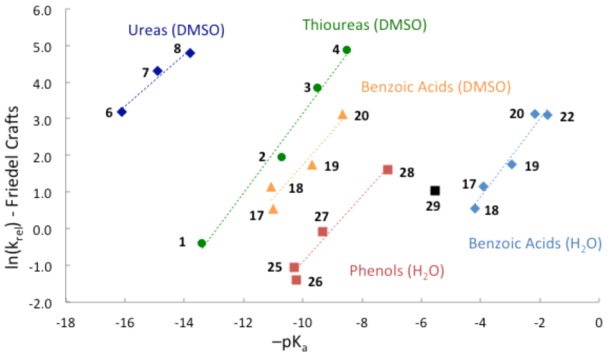

Figure 12. Brønsted catalysis plot for the Friedel–Crafts reaction demonstrating LFERs for closely related catalyst groups.

Table 5. Brønsted α-Values for Different Catalyst Structural Types from Figures 11 and 12

		α	
catalyst series	solvent	Diels–Alder	Friedel–Crafts
Thioureas	DMSO	0.41	0.47
Ureas	DMSO	-	0.31
Benzoic Acids	DMSO	-	0.39
Benzoic Acids	H_2O	0.57	0.46
Phenols	H_2O	0.39	0.39

would be predicted to provide much higher activity. In practice, the opposite is observed where ureas exhibited greater (**6**, **7** vs **2**, **3**) or similar (**8** vs **4**) activation of the nitro group compared to their thiourea analogues, despite the much greater acidity of the thioureas (4–5 orders of magnitude difference). Highly reactive catalysts not belonging to a clearly defined series, including common Brønsted acids, are included in Figure 11 and further highlight the disparity between acidity and activity. Interestingly, Takenaka's azaindolium catalyst **14** displayed much higher activity than PPTS, despite similar acidities and similar pyridinium–H donor moieties. Taken together, these observations reinforce the risks of using pK_a measurements to estimate reactivity.

3. CONCLUSIONS

In conclusion, a sensor is described that provides an assessment of the reactivity over 3–4 orders of magnitude for 33 hydrogen-bonding catalysts. Useful correlations are obtained between the wavelength shifts that catalysts cause to the pyrazinone sensor and the rate-determining steps in Diels–Alder and Friedel–Crafts reactions. As a result, only the wavelength shifts upon saturation of the sensor with catalysts need to be measured vs the more time-consuming titration studies. Consequently, the sensor may also find use as a rapid means for measuring pK_a values in series of related compounds.

In contrast to established acidity (pK_a) values, the sensor wavelength shift is a highly predictive metric for the relative reactivity of catalysts encompassing a broad range of structures and strengths. Notable acidity-activity disparities include cationic catalysts (low acidity, high reactivity), and benzoic acids (high acidity, low reactivity), the strengths of which are more accurately gauged by their interaction with the sensor. Overall, the sensor is a superior surrogate for the diverse electrophiles (enone and nitroalkene) used compared to water and is better able to assess secondary interactions. The data collected was used to formulate the relationship described in eq 3, which provides a direct means of assessing the reactivity of a catalyst in a given reaction using the sensor signal. The resulting parameters also reveal relationships between substrate•catalyst binding, catalyst-induced LUMO-lowering, and catalyst structure.

Investigation of additional catalyzed reactions with the sensor, empirically or computationally, has the potential to expand eq 3 to achieve quantitative predictive power across a large range of reaction platforms and catalysts (hydrogen bonding, Brønsted acid, and Lewis acid). Further studies to achieve this goal are underway.

■ ASSOCIATED CONTENT

Ⓢ Supporting Information

Experimental procedures, characterization of new compounds, UV-titration data, and Diels–Alder and Friedel–Crafts rate data. This material is available free of charge via the Internet at http://pubs.acs.org.

■ AUTHOR INFORMATION

Corresponding Author

marisa@sas.upenn.edu

Notes

The authors declare no competing financial interest.

■ ACKNOWLEDGMENTS

We are grateful to NIH (GM-087605) for financial support of this research. Partial instrumentation support was provided by the NIH for MS (1S10RR023444) and NMR (1S10RR022442). Thanks to Christian Schafmeister (Temple University) for donations of catalyst **24** and to Anita Mattson (Ohio State University) for **9** and **32**. We are indebted to Drs. George Furst and Jun Gu (UPenn) for NMR assistance. Dr. Osvaldo Gutierrez and Sergei Tcyrulnikov (UPenn) are acknowledged for helpful discussions. We thank Ms. Kaila Orlandini for UV-titration experiments.

■ REFERENCES

(1) (a) Taylor, M. S.; Jacobsen, E. N. *Angew. Chem., Int. Ed.* **2006**, *45*, 1520–1543. (b) Doyle, A. G.; Jacobsen, E. N. *Chem. Rev.* **2007**, *107*, 5713–5743. (c) Akiyama, T. *Chem. Rev.* **2007**, *107*, 5744–5758. (d) Schreiner, P. R. *Chem. Soc. Rev.* **2003**, *32*, 289–296. (e) Akiyama, T.; Itoh, J.; Fuchibe, K. *Adv. Synth. Catal.* **2006**, *348*, 999–1010. (f) Connon, S. J. *Synlett* **2009**, 354–376. (g) Takemoto, Y. *Chem. Pharm. Bull.* **2010**, *58*, 593–601. (h) Sohtome, Y.; Nagasawa, K. *Synlett* **2010**, 1–22. (i) Schenker, S.; Zamfir, A.; Freund, M.; Tsogoeva, S. B. *Eur. J. Org. Chem.* **2011**, 2209–2222. (j) Auvil, T. J.; Schafer, A. G.; Mattson, A. E. *Eur. J. Org. Chem.* **2014**, 2633–2646.

(2) Select examples: (a) Aleman, J.; Parra, A.; Jiang, H.; Jørgensen, K. A. *Chem.—Eur. J.* **2011**, *17*, 6890–6899 and references therein. (b) Okino, T.; Hoashi, Y.; Takemoto, Y. *J. Am. Chem. Soc.* **2003**, *125*, 12672–12673. (c) Hoashi, Y.; Okino, T.; Takemoto, Y. *Angew. Chem., Int. Ed.* **2005**, *44*, 4032–4035. (d) Herrera, R. P.; Sgarzani, V.; Bernardi, L.; Ricci, A. *Angew. Chem., Int. Ed.* **2005**, *44*, 6576–579. (e) Vakulya, B.; Varga, S.; Csampai, A.; Soos, T. *Org. Lett.* **2005**, *7*, 1967–1969. (f) Zuend, S. J.; Jacobsen, E. N. *J. Am. Chem. Soc.* **2007**, *129*, 15872–15883. (g) Connon, S. J. *Chem. Commun.* **2008**, 2499–2510.

(3) Fukuzumi parameters: (a) Fukuzumi, S.; Ohkubo, K. *Chem.—Eur. J.* **2000**, *6*, 4532–4535. (b) Fukuzumi, S.; Ohkubo, K. *J. Am. Chem. Soc.* **2002**, *124*, 10270–10271.

(4) Irving-Williams order: (a) Irving, H.; Williams, R. J. P. *Nature* **1948**, *162*, 746–747. (b) Irving, H.; Williams, R. J. P. *J. Chem. Soc.* **1953**, 3192–3210.

(5) Breugst, M.; Gree, R.; Houk, K. N. *J. Org. Chem.* **2013**, *78*, 9892−9897.
(6) Gilli, P.; Pretto, L.; Bertolasi, V.; Gilli, G. *Acc. Chem. Res.* **2009**, *42*, 33−44.
(7) (a) Annamalai, V. R.; Linton, E. C.; Kozlowski, M. C. *Org. Lett.* **2009**, *11*, 621−624. (b) Tuerkmen, Y. E.; Rawal, V. H. *J. Org. Chem.* **2013**, *78*, 8340−8353. (c) Shokri, A.; Wang, Y.; O'Doherty, G. A.; Wang, X.-B.; Kass, S. R. *J. Am. Chem. Soc.* **2013**, *135*, 17919−17924. (d) Beletskiy, E. V.; Schmidt, J.; Wang, X.-B.; Kass, S. R. *J. Am. Chem. Soc.* **2012**, *134*, 18534−18537.
(8) Huynh, P. N. H.; Walvoord, R. R.; Kozlowski, M. C. *J. Am. Chem. Soc.* **2012**, *134*, 15621−15623.
(9) Steiner, T. *Angew. Chem., Int. Ed.* **2002**, *41*, 48−76.
(10) (a) Deters, J. F.; McCusker, P. A.; Pilger, R. C., Jr. *J. Am. Chem. Soc.* **1968**, *90*, 4583−4585. (b) Hilt, G.; Puenner, F.; Moebus, J.; Naseri, V.; Bohn, M. A. *Eur. J. Org. Chem.* **2011**, 5962−5966 and references therein.
(11) For a relevant example of monitoring hydrogen-bonding interactions with stronger thiourea catalysts, see: Lippert, K. M.; Hof, K.; Gerbig, D.; Ley, D.; Hausmann, H.; Guenther, S.; Schreiner, P. R. *Eur. J. Org. Chem.* **2012**, 5919−5927.
(12) (a) Nakai, S.; Yasui, M.; Nakazato, M.; Iwasaki, F.; Maki, S.; Niwa, H.; Ohashi, M.; Hirano, T. *Bull. Chem. Soc. Jpn.* **2003**, *76*, 2361−2387. (b) Sekiguchi, T.; Maki, S.; Niwa, H.; Ikeda, H.; Hirano, T. *Tetrahedron Lett.* **2004**, *45*, 1065−1069. (c) Takamuki, Y.; Maki, S.; Niwa, H.; Ikeda, H.; Hirano, T. *Chem. Lett.* **2004**, *33*, 1484−1485. (d) Takamuki, Y.; Maki, S.; Niwa, H.; Ikeda, H.; Hirano, T. *Tetrahedron* **2005**, *61*, 10073−10080. (e) Hirano, T.; Sekiguchi, T.; Hashizume, D.; Ikeda, H.; Maki, S.; Niwa, H. *Tetrahedron* **2010**, *66*, 3842−3848.
(13) See Supporting Information for additional experimental details.
(14) Huang, Y.; Unni, A. K.; Thadani, A. N.; Rawal, V. H. *Nature* **2003**, *424*, 146.
(15) (a) Schafer, A. G.; Wieting, J. M.; Mattson, A. E. *Org. Lett.* **2011**, *13*, 5228−5231. (b) Schafer, A. G.; Wieting, J. M.; Fisher, T. J.; Mattson, A. E. *Angew. Chem., Int. Ed.* **2013**, *52*, 11321−11324.
(16) Tran, N. T.; Wilson, S. O.; Franz, A. K. *Org. Lett.* **2012**, *14*, 186−189.
(17) For additional reports investigating silanol and silanediol catalysis see: (a) Kondo, S.-I.; Harada, T.; Tanaka, R.; Unno, M. *Org. Lett.* **2006**, *8*, 4621−4624. (b) Tran, N. T.; Min, T.; Franz, A. K. *Chem.—Eur. J.* **2011**, *17*, 9897−9900. (c) Liu, M.; Tran, N. T.; Franz, A. K.; Lee, J. K. *J. Org. Chem.* **2011**, *76*, 7186−7194. (d) Wilson, S. O.; Tran, N. T.; Franz, A. K. *Organometallics* **2012**, *31*, 6715−6718. (e) Min, T.; Fettinger, J. C.; Franz, A. K. *ACS Catal.* **2012**, *2*, 1661−1666. (f) Beemelmanns, C.; Husmann, R.; Whelligan, D. K.; Ozcubukcu, S.; Bolm, C. *Eur. J. Org. Chem.* **2012**, 3373−3376. (g) Tran, N. T.; Wilson, S. O.; Franz, A. K. *Chem. Commun.* **2014**, *50*, 3738−3740.
(18) Parker, M. F. L.; Osuna, S.; Bollot, G.; Vaddypally, S.; Zdilla, M. J.; Houk, K. N.; Schafmeister, C. E. *J. Am. Chem. Soc.* **2014**, *136*, 3817−3827.
(19) (a) Wittkopp, A.; Schreiner, P. R. *Chem.—Eur. J.* **2003**, *9*, 407−414. (b) Schreiner, P. R. *Chem. Soc. Rev.* **2003**, *32*, 289−296.
(20) (a) Connon, S. J. *Chem.—Eur. J.* **2006**, *12*, 5418−5427. (b) Takemoto, Y. *Org. Biomol. Chem.* **2005**, *3*, 4299−4306. (c) Tan, B.; Hernandez-Torres, G.; Barbas, C. F., III. *J. Am. Chem. Soc.* **2011**, *133*, 12354−12357.
(21) (a) So, S. S.; Burkett, J. A.; Mattson, A. E. *Org. Lett.* **2011**, *13*, 716−719. (b) So, S. S.; Mattson, A. E. *J. Am. Chem. Soc.* **2012**, *134*, 8798−8801. (c) So, S. S.; Auvil, T. J.; Garza, V. J.; Mattson, A. E. *Org. Lett.* **2012**, *14*, 444−447. (d) Auvil, T. J.; So, S. S.; Mattson, A. E. *Angew. Chem., Int. Ed.* **2013**, *52*, 11317−11320. (e) Hardman, A. M.; So, S. S.; Mattson, A. E. *Org. Biomol. Chem.* **2013**, *11*, 5793−5797. (f) So, S. S.; Oottikkal, S.; Badjic, J. D.; Hadad, C. M.; Mattson, A. E. *J. Org. Chem.* **2014**, *79*, 4832−4842.
(22) Takenaka, N.; Sarangthem, R. S.; Seerla, S. K. *Org. Lett.* **2007**, *9*, 2819−2822.
(23) (a) Rodriguez, A. A.; Yoo, H.; Ziller, J. W.; Shea, K. J. *Tetrahedron Lett.* **2009**, *50*, 6830−6833. (b) Borovika, A.; Tang, P.-I.; Klapman, S.; Nagorny, P. *Angew. Chem., Int. Ed.* **2013**, *52*, 13424−13428. (c) Cranwell, P. B.; Hiscock, J. R.; Haynes, C. J. E.; Light, M. E.; Wells, N. J.; Gale, P. A. *Chem. Commun.* **2013**, *49*, 874−879.
(24) The use of a chiral thiophosphorodiamide catalyst for an asymmetric addition of naphthoquinones into β-nitrostyrenes has been described: Wu, R.; Chang, X.; Lu, A.; Wang, Y.; Wu, G.; Song, H.; Zhou, Z.; Tang, C. *Chem. Commun.* **2011**, *47*, 5034−5036.
(25) Select examples of squaramide-based organocatalysis: (a) Malerich, J. P.; Hagihara, K.; Rawal, V. H. *J. Am. Chem. Soc.* **2008**, *130*, 14416−14417. (b) Zhu, Y.; Malerich, J. P.; Rawal, V. H. *Angew. Chem., Int. Ed.* **2010**, *49*, 153−156. (c) Konishi, H.; Lam, T. Y.; Malerich, J. P.; Rawal, V. H. *Org. Lett.* **2010**, *12*, 2028−2031. (d) Yang, W.; Du, D.-M. *Org. Lett.* **2010**, *12*, 5450−5453. (e) Qian, Y.; Ma, G.; Lv, A.; Zhu, H.-L.; Zhao, J.; Rawal, V. H. *Chem. Commun.* **2010**, *46*, 3004−3006. (f) Yang, W.; Yang, Y.; Du, D.-M. *Org. Lett.* **2013**, *15*, 1190−1193. (g) Manoni, F.; Connon, S. J. *Angew. Chem., Int. Ed.* **2014**, *53*, 2628−2632.
(26) Barlin, G. B.; Brown, D. J.; Kadunc, Z.; Petric, A.; Stanovnik, B.; Tisler, M. *Aust. J. Chem.* **1983**, *36*, 1215−1220.
(27) The parameter σ_o^i was used to account for *ortho* electronic influences: Pytela, O.; Liska, J. *Collect. Czech. Chem. Commun.* **1994**, *59*, 2005−2021.
(28) (a) Shokri, A.; Wang, X.-B.; Kass, S. R. *J. Am. Chem. Soc.* **2013**, *135*, 9525−9530. (b) Fleming, E. M.; McCabe, T.; Connon, S. J. *Tetrahedron Lett.* **2006**, *47*, 7037−7042. (c) Zhuang, W.; Hazell, R. G.; Jørgensen, K. A. *Org. Biomol. Chem.* **2005**, *3*, 2566−2571. (d) Lancianesi, S.; Palmieri, A.; Petrini, M. *Chem. Rev.* **2014**, *114*, 7108−7149 and references therein.
(29) Jencks, W. P.; Regenstein, J. Ionization Constants of Acids and Bases. In *CRC Handbook of Biochemistry and Molecular Biology*, 3rd ed.; Fassman, G. D., Ed.; CRC Press: Cleveland, OH, 1975; Vol. *1*, pp 305−351.
(30) Huang, H.; Jacobsen, E. N. *J. Am. Chem. Soc.* **2006**, *128*, 7170−7171.
(31) Bordwell, F. G. *Acc. Chem. Res.* **1998**, *21*, 456−463.
(32) Belokon, Y. N.; Harutyunyan, S.; Vorontsov, E. V.; Peregudov, A. S.; Chrustalev, V. N.; Kochetkov, K. A.; Pripadchev, D.; Sagyan, A. S.; Beck, A. K.; Seebach, D. *ARKIVOC* **2004**, 132−150.
(33) Pandiaraju, S.; Chen, G.; Lough, A.; Yudin, A. K. *J. Am. Chem. Soc.* **2001**, *123*, 3850−3851.
(34) Birchall, J. M.; Haszeldine, R. N.; Parkinson, A. R. *J. Chem. Soc.* **1961**, 2204−2206.
(35) Haynes, W. M., Ed. Dissociation Constants of Organic Acids and Bases. In *CRC Handbook of Chemistry and Physics*, 94th ed.; CRC Press: Boca Raton, FL, 2013.
(36) Uyeda, C.; Jacobsen, E. *J. Am. Chem. Soc.* **2008**, *130*, 9228−9229.
(37) Koppel, I.; Koppel, J.; Leito, I. *J. Phys. Org. Chem.* **1996**, *9*, 265−268.
(38) (a) Jensen, K. H.; Sigman, M. S. *J. Org. Chem.* **2010**, *75*, 7194−7201. (b) Jensen, K. H.; Sigman, M. S. *Angew. Chem., Int. Ed.* **2007**, *46*, 4748−4750. (c) Nickerson, D. M.; Angeles, V. V.; Auvil, T. J.; So, S. S.; Mattson, A. E. *Chem. Commun.* **2013**, *49*, 4289−4291.
(39) Li, X.; Deng, H.; Zhang, B.; Li, J.; Zhang, L.; Luo, S.; Cheng, J.-P. *Chem.—Eur. J.* **2010**, *16*, 450−455.
(40) (a) Hine, J.; Linden, S.-M.; Kanagasabapathy, V. M. *J. Am. Chem. Soc.* **1985**, *107*, 1082−1083. (b) Hine, J.; Linden, S.-M.; Kanagasabapathy, V. M. *J. Org. Chem.* **1985**, *50*, 5096−5097.
(41) Jakab, G.; Tancon, C.; Zhang, Z.; Lippert, K. M.; Schreiner, P. R. *Org. Lett.* **2012**, *14*, 1724−1727.
(42) Ni, X.; Li, X.; Wang, Z.; Cheng, J.-P. *Org. Lett.* **2014**, *16*, 1786−1789. (b) Kaupmees, K.; Tolstoluzhsky, N.; Raja, S.; Rueping, M.; Leito, I. *Angew. Chem., Int. Ed.* **2013**, *52*, 11569−11572.
(43) Carey, F. A.; Sundberg, R. J. *Advanced Organic Chemistry, Part A: Structure and Mechanisms*, 5th ed.; Springer: New York, 2007; pp 348−354.

(44) Values of $\ln(k_{rel})$ are plotted for continuity in Figures 11 and 12. Numerical α value listed in the text were obtained from plots of $\log(k_{rel})$ in accord with eq 4.
(45) Harper, K. C.; Sigman, M. S. *J. Org. Chem.* **2013**, *78*, 2813−2818.